

Interference-Aware Path Planning Optimization for Multiple UAVs in Beyond 5G Networks

Jongyul Lee and Vasilis Friderikos

Abstract—Integrating unmanned aerial vehicles (UAVs) as flying base stations (FBSs) is expected to be an important architectural element in the beyond 5G/6G mobile wireless networks. A key operational aspect in UAV-aided 5G/6G networks is the UAV path optimization (or trajectory planning as it is also commonly referred to). In this paper, we address this problem using a mixed integer linear programming (MILP) formulation for FBS path optimization in terms of traveling time considering co-channel interference and time windows in serving ground users (GUs) at cluster points (CPs) for constructing the multiple UAV paths in both a single-cell and a multi-cell wireless network. In the proposed technique, we assume that all FBSs depart and return to a single depot, which is considered to be a terrestrial 5G/6G base station (BS). The novelty of the proposed solution compared to previous techniques is that we take explicitly into account the interference under the unit disk graph (UDG) model to create interference-aware UAV's trajectory. Numerical investigations reveal that the proposed interference-aware path optimization approaches improve the overall performance of the network up to approximately 21% in terms of throughput for the FBSs. Notably, these gains come with an unnoticeable increase in the total completion time, which is comparable to well-known previously proposed solutions. Additionally, the proposed heuristic algorithms provide competitive decision making with low underlying computational complexity rendering them amenable for real-time implementation.

Index Terms—Flying base station (FBS), interference model, mixed integer linear programming (MILP), multi-cell, path planning, unit disk graph (UDG), unmanned aerial vehicle (UAV).

I. INTRODUCTION

IN the upcoming sixth-generation (6G) networks, it is envisioned that the use of unmanned aerial vehicles (UAVs)¹ in the form of flying (mobile) base station (FBS)² will play a significant role in augmenting the existing terrestrial wireless network operations in a plethora of different use cases such as information dissemination, on-demand hot spot data coverage and data collection for Internet of things (IoTs) [2]–[7]. Different types of events in urban or hot spot areas where a large number of users flock, e.g., a stadium, festival, parade, etc., might create severe congestion episodes on the network

Manuscript received August 31, 2021; revised December 29, 2021; approved for publication by Hongliang Zhang, Guest Editor, January 29, 2022.

This research work was presented in part at the IEEE Wireless Communications and Networking Conference (WCNC), May 25–28, 2020, [1].

The authors are with the Department of Engineering, Centre of Telecommunication Research, King's College London, London, WC2R 2LS, U.K, e-mail: jongyul.lee@kcl.ac.uk, vasilis.friderikos.kcl.ac.uk

J. Lee is the corresponding author.

Digital Object Identifier: 10.23919/JCN.2022.000006

¹Frequently used abbreviations are summarized in Table I.

²Hereafter, the terms of 'UAV' and 'FBS' are used interchangeably in the paper.

due to a concurrent high data demand that needs to be served by the fixed cellular network infrastructure. In such use case scenarios, UAV-assisted 5G/6G networks can boost network efficiency and flexibility by providing seamless on-demand ultra high capacity connectivity for elastic traffic in those areas. Moreover, FBSs can complement other areas beyond the coverage area of a terrestrial base station (BS) and support the existing ground-based heterogeneous network (HetNet) owing to their flexible 3D movement [2], [3]. Specifically, in a rural setting, it is easier for the FBS to reach areas with poor network coverage signal in agriculture, industry factories, construction zones, isolated areas, etc. In other words, the FBS can provide intelligent offloading of the data demand, which has a strong spatio-temporal correlation and seamless connectivity between source and destination [8]–[11]. However, these benefits come with a price in which the deployment of the FBS suffers from energy consumption due to its limited battery life when conducting the aforementioned assistance to the fixed network infrastructure. Therefore, some of the most challenging aspects in the deployment of the FBS have been recently paid attention related to reducing the energy with respect to minimizing consumed time (traveling time), optimizing trajectory planning and transmit power control, and maximizing data rate [9], [10]. However, little attention has been placed in orchestrating the trajectories of multiple FBSs, taking into account interference so that possible rendezvous points of the FBSs can be eliminated as the FBSs serve ground users (GUs), which will result in a substantial reduction of co-channel interference.

A. Related Work

The prior works in [12]–[17] proposed the deployment of UAVs as FBSs that use terrestrial BSs as a depot. In that case, FBSs depart for serving GUs and then return to the original BS (depot) after completing the service where battery re-charging can take place since UAVs are powered by onboard battery packs that can provide limited energy.

In the UAV-aided 5G/6G wireless network, a crucial aspect that need to be addressed is the UAV trajectory planning that determines the traveling (flying) path to serve different GUs. This is crucially important since the trajectory planning determines the overall traveling time, delivered service to the GUs, and the consumed energy from UAV [10]. The UAV trajectory planning optimization problem resembles the well-known traveling salesman problem (TSP) [16], [18], [19], as well as the vehicle routing problem (VRP) [17], [20]–[22]. To this end, various different TSP and VRP types of optimization

Creative Commons Attribution-NonCommercial (CC BY-NC).

This is an Open Access article distributed under the terms of Creative Commons Attribution Non-Commercial License (<http://creativecommons.org/licenses/by-nc/3.0>) which permits unrestricted non-commercial use, distribution, and reproduction in any medium, provided that the original work is properly cited.

models have been previously used to address the trajectory optimization problem in a spatially large distributed area. To put things in context, under the TSP/VRP context, a traveler or vehicle (in this case, a UAV) aims to find the lowest cost route in terms of distance so that it can visit all locations once and return to the origin (the depot; which in this case is the terrestrial BS); TSP and VRP are well-known NP-hard problems [23], and hence, both suffer from the curse of dimensionality which means that it is highly problematic to efficiently solve medium to large network instances.

Interference avoidance and mitigation pertain to the problem of concurrent multiple wireless transmissions using the same channel (co-channel interference). It is of fundamental importance in the design of wireless mobile communications since these networks are, in essence, interference limited. Various works [24]–[33] have addressed interference coordination in the deployment of UAVs in wireless networks. In particular, the works in [24]–[30] have studied the UAV’s trajectory to mitigate the interference. Moreover, a number of previous works [24]–[33] have particularly focused on the issue of power control coordination to improve the aggregate throughput of UAVs.

As a way to enhance the overall performance of the network, it is foreseeable to deploy multiple FBSs so that they cooperatively serve GUs whilst fulfilling quality of service (QoS) constraints in terms of serving time windows. Furthermore, since the FBS’s onboard energy is considerably limited, they require a terrestrial macro cellular BS acting as a depot, where the FBSs are dispatched and return, which provides the necessary mechanism for the FBS to recharge in order to continue their missions. Despite the fact that this can be deemed as a critical aspect in creating an efficient FBS deployment, only a few studies have focused on this use case scenario [16], [17], [22].

B. Motivation and Contributions

Significant levels of co-channel interference can occur³ in the case of a single-cell and multiple FBSs simultaneously serving GUs in close spatial proximity. This scenario can be generalized for a typical multi-cell wireless network, where FBSs might create critical levels of interference in neighbor cells, i.e., interference between respective GUs at the edge cells caused by the FBSs dispatched from neighbor respective BSs. For the case of a large number of neighboring cells, the network will inevitably require large-scale multi-cell cooperation in order to improve its performance [11]. This motivates the investigation of interference-aware path planning optimization schemes for multiple FBSs in a multi-cell network.

To the best of our knowledge, this is the first work in the design of optimal trajectory planning of multiple FBSs hosted at a terrestrial BS that amalgamates the following aspects in an explicit manner:

³A simple, albeit inefficient, the technique would be to partition radio resources so that different FBSs use orthogonal frequency resources. However, in this paper, to increase spectral efficiency, we assume that all FBSs use the same frequency resources, which is the most challenging use case scenario.

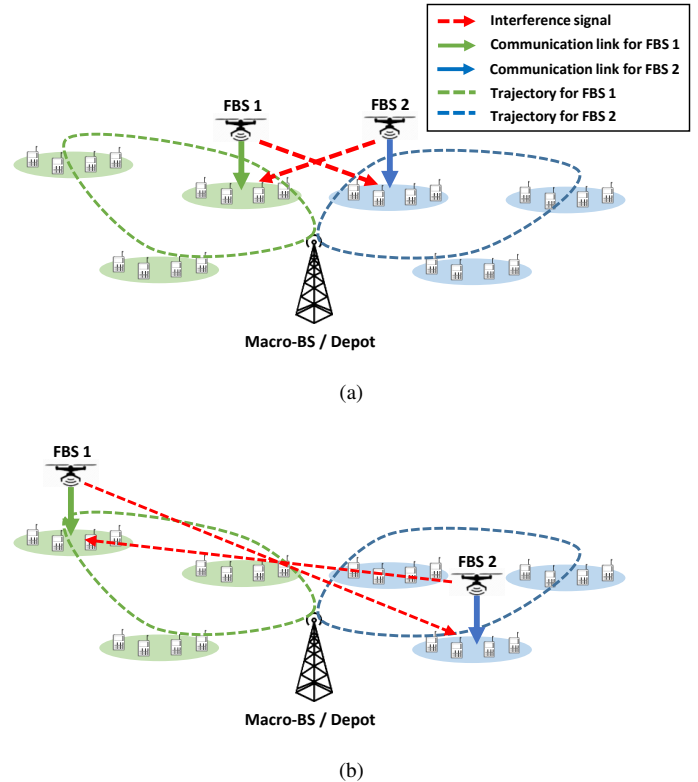


Fig. 1. The effect of FBS trajectory on interference when UAVs serve GUs at CPs. (a) A trajectory with strong interference occurrence in close proximity. (b) Interference avoidance by a trajectory design where FBSs serving GUs at CPs in close proximity is eliminated.

- Interference-aware trajectory planning optimization framework for multiple FBSs using a Hamiltonian path-based formulation in a large distributed area.
- Interference awareness under the unit disk graph (UDG) model; a model that has been widely used in the literature due to its ability to capture interference between adjacent transmitting nodes [34]–[36], but has not yet been previously applied in the domain of UAV-aided mobile networks.
- QoS support by modeling time windows to serve different GUs clustered at other different locations in a single/multi-macro cell network.
- Multiple FBSs deployment from the same macro BS or neighbour macro BSs in a single/multi-macro cell wireless network.

Fig. 1 illustrates the effect of FBS trajectory planning design in reducing interference levels when multiple FBSs serve GUs in a defined area. It is important to highlight that previous, closely related, research works [24]–[33] focused on interference mitigation via transmit power control for a set of links between a UAV and a set of served GUs or terminals, most closely resembling the case shown in Fig. 1(a). However, as illustrated in Fig. 1(b), our proposed interference-aware FBS trajectory planning scheme does not in essence allow that FBSs simultaneously serve GUs at close proximity; hence our focus is complementary to previous research works. In that respect, interference levels can be dramatically reduced and

a less strict power control scheme can be utilized due to that reason. Therefore, our proposed scheme using the UDG model and integrated time variables allows for an efficient spatio-temporal orchestration of the FBSs so that overall network performance is increased. Furthermore, as already eluded, note that the proposed work is complementary with previous works since interference mitigation techniques (power control) can still be applied when an FBS hovers to serve a set of GUs. However, our emphasis is on interference avoidance which can allow simple power control techniques to be sufficient, such as fractional power control. This will result in reducing control plane overhead and increase scalability.

Moreover, the prior works [24]–[33] did not consider interference between different clusters of GUs distributed in a wireless macro-cell setting. More specifically, prior works [24]–[30] proposed an UAV trajectory optimization to mitigate interference; however, these works did not consider the provision for optimal path planning design with multiple FBSs via a Hamiltonian path like formulation problem [23]. This is a critical differentiation since such an approach is appropriate to the large macro-cell scenario while at the same time taking into account specific QoS constraints in terms of time windows for serving GUs. Likewise, our focus on optimizing multiple FBSs residing at different macro-BS is considered to reflect a multi-cell network setting. On that frontier, few prior works [37]–[39] have studied the UAV deployment related to a nominal multi-cell wireless network, i.e., multiple depots.

The contributions and the novelties of this paper can be summarized as follows:

- We formulate a novel multiple FBSs trajectory planning optimization problem using a mixed integer linear programming (MILP) by explicitly taking into account interference with the UDG model that avoids the interference by establishing a circular graph. The proposed formulation explicitly models time windows for FBSs serving different clusters that allow different levels of service to be implemented. The goal of the problem is to minimize FBS travel time while increasing overall network capacity in the network.
- With the FBSs trajectory planning optimization problem, we consider use case scenarios representing both a single-cell and a typical multi-cell network where inter-cell interference causes a detrimental effect, especially for GUs located at the cell edge. Hence, the proposed trajectory planning optimization provides novel cell boundaries that have not been previously reported in the multi-cell network case by adopting an auxiliary variable [1] that enables FBS routes to be within a given cell. Since the optimization problem is inherently a mixed integer non-linear programming (MINLP), it is linearized by elimination product of variables [40].
- An interference-aware FBS trajectory planning heuristic algorithm is developed using the UDG model. The proposed heuristic algorithm is based on local search techniques (LSTs) [16], [41], which enables scalability with a competitive performance whilst having a low computational complexity compared to the optimal solutions.
- Finally, meticulous numerical investigations are presented

TABLE I
MAJOR NOTATIONS AND ACRONYMS USED THROUGHOUT THE PAPER.

Abbreviation & Notation	Definition
AAT	Average achievable throughput
CP	Cluster point
FBS	Flying base station
GU	Ground user
LST	Local search techniques
MILP	Mixed integer linear programming
SINR	Signal to interference plus noise ratio
TTT	Total traveling time of all FBSs
UDG	Unit disk graph
OUT-x (S/M)	Optimal UAV trajectory planning in single/multi-cell network
OUT-xIA (SIA/MIA)	Optimal UAV trajectory planning in single/multi-cell network with interference awareness
HUT-x (S/M)	Heuristic UAV trajectory planning in single/multi-cell network
HUT-xIA (SIA/MIA)	Heuristic UAV trajectory planning in single/multi-cell network with interference awareness
\mathcal{V}	Set of vertices
\mathcal{V}_d	Set of BSs (depots)
\mathcal{V}_c	Set of CPs
\mathcal{K}	Set of UAVs (FBSs)
\mathcal{C}	Set of cells
θ_r	Unit disk graph (UDG) radius
x_{ijk}	Decision variable for given vertex i , j and FBS k
z_{ijk}	Decision variable for given vertex i , j and FBS k
s_i	Service time that an FBS consumes at CP i
w_i	Arrival time of an FBS at CP i
t_{ij}	Traveling time of an FBS from vertex i to vertex j
d_{ij}	Distance between vertex i and vertex j
v	Velocity of the FBS
δ_i	Limited number of FBSs that depart and return to BS i
e_0	Mission start time
l_0	Maximum window time
λ	Sufficiently large integer number
q_{ijd}	Auxiliary variable that creates feasible or infeasible FBS routes for given vertex i , j and cell d
y_{ij}	Decision variable for given vertex i , j
ψ	Set of two CPs that fall within the interference range under the UDG model
Ψ	Set of ψ
ID-UDG $_i$	Interference detection for given CP i
\mathbb{U}	Number of ID-UDG
OE $_i$	Outage event for given CP i
\mathbb{E}	Number of OE
SINR $_i$	Signal-to-interference-plus-noise ratio at CP i
γ_{th}	SINR threshold
i, j	Index of vertices
k	Index of FBSs

via a large number of Monte Carlo simulations to validate the performance of the proposed designs. It is shown that the proposed set of solutions that explicitly embrace interference awareness outperform other benchmark schemes. The proposed approaches achieve a higher aggregate throughput with only a slight loss of travel time than that of the benchmarks.

Notation: The notation used throughout the paper is reported in Table I.

II. SYSTEM MODEL

A. Scenario

The underlying scenario of the UAV-assisted 5G/6G network is depicted in Figs. 1 and 3, which includes the operational procedure of multiple FBSs hosted at a single terrestrial BS. The different steps in deploying FBSs are briefly described below,

- Without loss of generality, one and three hexagon cells are considered in the form of a single-cell and a multi-cell network, respectively. Via front-haul links, the cells are connected to the wireless access network and relevant cloud-based radio resource controllers where UAV orchestration occurs.
- A set of FBSs resides in a 5G/6G terrestrial macro BS that acts as a depot at the center of each cell. All FBSs are dispatched from a BS and visit all assigned CPs to serve GUs. Then, they return to the (same) BS in order to (re)charge their battery/(re)fuel.
- A cluster point (CP) is defined as the epicenter in the cluster of GUs as shown in Fig. 3. An FBS overflies and hovers at the CP to serve the GUs. A set of CPs are randomly distributed within a pre-determined geographical area in both the single-cell and the multi-cell network setting. The location of all CPs is shared with all BSs through the cloud controllers.
- A single FBS only serves each CP. The FBS starts to serve GUs via a downlink transmission scenario by hovering once arriving at the serving CP.
- The FBS equally serves those GUs for a pre-defined time period, which is called as the service time.
- Once the service is completed, an FBS moves to the next CP. When the FBS visited all assigned CPs, it returns to the macro-BS to offload collected data.

B. Network Model

Hereafter, without loss of generality, we assume that FBSs fly with constant velocity denoted as v and utilize the same altitude denoted as h . To fix ideas, the aforementioned UAV-assisted 5G/6G network is modeled as an undirected graph $\mathcal{G} = (\mathcal{V}, \mathcal{A})$, where $\mathcal{V} = \mathcal{V}_c \cup \mathcal{V}_d$. $\mathcal{V}_c = \{1, 2, \dots, N\}$ denotes the set of CPs and $\mathcal{V}_d = \{1, 2, \dots, M\}$ denotes the set of depots (BSs) in 2-dimensional Cartesian coordinate system. $\mathcal{A} = \{(i, j) : i, j \in \mathcal{V}, i \neq j\}$ is the set of links (routes) which is defined as d_{ij} , i.e., the Euclidean distance. The travel time that FBSs travel between vertices including CPs and a BS is denoted as t_{ij} and it can be calculated by using the distance of the link with the FBS velocity v , i.e., $t_{ij} = d_{ij}/v$. The set of FBSs is denoted by $\mathcal{K} = \{1, 2, \dots, K\}$. $\mathcal{C} = \{1, 2, \dots, C\}$ indicates the set of cells, each of which includes a single BS and several CPs. CP i has time window $[e_i, l_i]$, where $e_i \leq l_i$, during which an FBS starts serving GUs at CP i . Let s_i be a constant service time when the FBS serves GUs to transmit data at CP i .

C. Air to Ground Channel Model

We adopt the most widely used air to ground channel model in order to calculate signal to interference plus noise ratio

(SINR) and estimate the achievable throughput in the network. As detailed in [42] and [43], a user receives three components of signals which are the line of sight (LoS), the strong reflected signals, i.e., none LoS (NLoS) and multiple reflected signals contributing to the so-called multi-path fading. The path loss for the NLoS signal is caused by the shadowing effect and reflection of signals from obstacles, the impact of which is higher than the LoS signal. In this paper, since we are interested in the average signal strength rather than the instantaneous one, we only consider the effects of the LoS and NLoS channel impairments for the air to ground channel model [44].

The path loss for LoS and NLoS links can be represented as follows [42], [44]:

$$L_{\text{LoS}} = 20 \log\left(\frac{4\pi f_c \sqrt{R^2 + h^2}}{c_l}\right) + \xi_{\text{LoS}}, \quad (1)$$

$$L_{\text{NLoS}} = 20 \log\left(\frac{4\pi f_c \sqrt{R^2 + h^2}}{c_l}\right) + \xi_{\text{NLoS}}, \quad (2)$$

where L_{LoS} and L_{NLoS} are the average path loss in dB for LoS and NLoS links. We assume that an FBS is located at an altitude h and GUs are randomly distributed within a maximum radius of R meters from a point (CP) corresponding to the projection of the FBS onto the ground as described in Fig. 2. In Eqs. (1) and (2), $\sqrt{\cdot}$ is expressed as the Euclidean distance between an FBS and a GU, and it indicates the elevation angle with respect to the GU. We consider the case where a GU is at a distant R from the point (CP) and the GU would be covered by two FBSs's transmit coverage as described in [44, Fig. 3]. c_l is the speed of light and f_c is the carrier frequency. In addition, ξ_{LoS} and ξ_{NLoS} denote the average additional loss to the free space propagation loss which relies on the environment. The probability of LoS connections at the elevation angle of $\tan^{-1}(h/R)$ can be written as [43],

$$\mathbb{P}_{\text{LoS}} = \frac{1}{1 + \alpha \exp(-\beta[\frac{180}{\pi} \tan^{-1}(h/R) - \alpha])}, \quad (3)$$

where α and β are constant values which depend on the environment, e.g., rural, urban, dense urban, etc. In addition to the above, the probability with respect to the NLoS component is expressed as $\mathbb{P}_{\text{NLoS}} = 1 - \mathbb{P}_{\text{LoS}}$.

Finally, the average path loss \bar{L} as a function of the altitude of the FBS and the radius of the coverage area is given as follows,

$$\bar{L} = \mathbb{P}_{\text{LoS}} \times L_{\text{LoS}} + \mathbb{P}_{\text{NLoS}} \times L_{\text{NLoS}}. \quad (4)$$

Given the above defined air to ground channel model, and assuming a constant transmit power P_t of an FBS k , then, the received power $P_{r,i,k}$ in dB at CP i on the ground terminal can be written as follows,

$$P_{r,i,k} = P_t - \bar{L}. \quad (5)$$

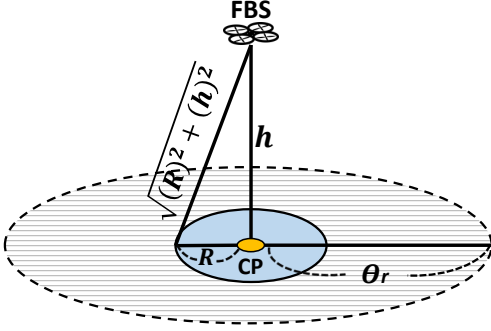


Fig. 2. The UDG model with the range θ_r and the transmission range R of an FBS.

D. UDG Model

UDG model has been widely used in the literature due to its ability to capture interference between adjacent transmitting nodes in a highly scalable and distributed manner [34]–[36]. This enables the design of efficient algorithms to create an interference disk graph where a set of nodes is connected by an edge if and only if their distance falls within a predefined interference range value. In this paper, the UDG model is described as a disk graph with a certain radius range denoted as θ_r from a point of an FBS which is vertically projection to the ground as illustrated in Fig. 2. The FBS travels with the UDG and it can detect other different UDGs traveled with the other FBSs once the UDG overlap the other UDGs (refer to Fig. 3(a)). Also, the location and coverage of UDGs are predictable given CPs and θ_r , because FBSs with the UDG visit and hover over all CPs until all service is completed. In other words, the overlapping UDGs traveled with FBSs are calculated by Euclidean distance between the FBSs in 2-dimension area, i.e., $d_{kk'} = d_{ij}$, $k, k' \in \mathcal{K}$, $i, j \in \mathcal{V}_c$.

E. Average Achievable Throughput Measurement

Similar to the work in (5), we evaluate the aggregate achievable throughput (AAT) and SINR value at CPs for multiple FBSs in order to estimate the performance of the network (this aspect is addressed in Section V in detail). Specifically, the achieved SINR can be written as follows,

$$\text{SINR}_{i,k} = \frac{P_{r,i,k}}{\sum_{k' \in \mathcal{K} \setminus \{k\}} P_{r,j,k'} + \mathcal{N}_0}, \quad \forall i, j \in \mathcal{V}_c, \quad \forall k \in \mathcal{K}, \quad (6)$$

where \mathcal{N}_0 denotes the white noise power. Thus, we yield the achievable throughput as follows:

$$\mathbb{C}_i \triangleq \sum_{u=1}^U B \Delta_{i,k,u} \log_2(1 + \text{SINR}_{i,k,u}), \quad \forall i \in \mathcal{V}_c, \quad \forall k \in \mathcal{K}, \quad (7)$$

where B indicates the transmit bandwidth which has been normalized to 1 Hz and $\text{SINR}_{i,k,u} \triangleq \text{SINR}_{i,k}$. Also, $\Delta_{i,k,u}$ represents a fractional time slot that can detect a simultaneous overlapping service time period, i.e., $s_i = \sum_{u=1}^U \Delta_{i,k,u}$, $\forall i \in$

\mathcal{V}_c , $\forall k \in \mathcal{K}$. Hence, the AAT in the network in terms of bps/Hz can be calculated as given by,

$$\text{AAT} = \frac{1}{N} \sum_{i \in \mathcal{V}_c} \mathbb{C}_i. \quad (8)$$

III. PROBLEM FORMULATION

A. UAV Trajectory Planning Formulation with Time Window and UDG Model in Cellular Networks

In this section, based on the discussed scenario and aforementioned system model, we address the proposed MILP formulation for path optimization with multiple FBSs while aiming to minimize the total FBS flying time with taking into account bounded cell setting. To this end, two decision variables of the model can be defined as follows,

$$x_{ijk} = \begin{cases} 1, & \text{if an FBS } k \text{ uses a link between} \\ & \text{vertex } i \text{ and vertex } j, \\ 0, & \text{otherwise,} \end{cases} \quad (9)$$

$$w_i = \text{arrival time at which service begins} \\ \text{at CP } i \text{ by FBS } k, \quad (10)$$

where x_{ijk} is binary and $w_i \geq 0$. We then enumerate several constraints to create an FBS trajectory and time window in the cell network as follows,

$$\sum_{\substack{i \in \mathcal{V} \\ (i \neq j)}} \sum_{k \in \mathcal{K}} x_{ijk} = 1, \quad \forall j \in \mathcal{V}, \quad (11a)$$

$$\sum_{j \in \mathcal{V}_c} \sum_{k \in \mathcal{K}} x_{ijk} \leq \delta_i, \quad \forall i \in \mathcal{V}_d, \quad (11b)$$

$$\sum_{\substack{j \in \mathcal{V} \\ (i \neq j)}} x_{jik} = \sum_{\substack{j \in \mathcal{V} \\ (i \neq j)}} x_{ijk}, \quad \forall k \in \mathcal{K}, \quad \forall i \in \mathcal{V}, \quad (11c)$$

$$x_{ijk} + x_{jik} \leq 1, \quad \forall k \in \mathcal{K}, \quad \forall i \in \mathcal{V}_d, \quad \forall j \in \mathcal{V}_c, \quad (11d)$$

The constraints in (11a)–(11d) relate to the FBS trajectory with multiple FBSs in both a single-cell and a multi-cell setting. The constraint in (11a) ensures that an FBS travels from a vertex i to a vertex j , i.e., the link between vertices. The constraint in (11b) ensures that the number of FBSs denoted as δ_i , which departs and return to BS i , is limited. The constraint in (11c) guarantees that an FBS leaves and arrives at a determined vertex. In other words, it guarantees flow conservation of the FBS route. The constraint in (11d) forces an FBS to visit more than two CPs⁵.

$$e_0 + t_{ij} \leq w_j + \lambda(1 - x_{ijk}), \quad \forall k \in \mathcal{K}, \quad \forall i \in \mathcal{V}_d, \quad \forall j \in \mathcal{V}_c \quad (12a)$$

$$w_i + s_i + t_{ij} \leq w_j + \lambda \left(1 - \sum_{k \in \mathcal{K}} x_{ijk}\right), \quad \forall i, j (i \neq j) \in \mathcal{V}_c \quad (12b)$$

⁴The word 'vertex' is used to include the expressions of both 'BS' and 'CP'.

⁵In this paper, we do not consider the trivial case of two CPs.

$$w_i + s_i + t_{ij} \leq x_{ijk}(l_0 - \lambda) + \lambda, \quad \forall k \in \mathcal{K}, \forall i \in \mathcal{V}_c, \forall j \in \mathcal{V}_d \quad (12c)$$

$$w_j \leq e_0 + t_{ij} + \lambda(1 - x_{ijk}), \quad \forall k \in \mathcal{K}, \forall i \in \mathcal{V}_d, \forall j \in \mathcal{V}_c \quad (12d)$$

$$w_j \leq w_i + s_i + t_{ij} + \lambda(1 - \sum_{k \in \mathcal{K}} x_{ijk}), \quad \forall i, j (i \neq j) \in \mathcal{V}_c \quad (12e)$$

$$e_i \leq w_i \leq l_i, \quad \forall i \in \mathcal{V}_c \quad (12f)$$

The constraints in (12a)–(12f) represent time window for the FBS trajectory planning. In the constraints, by utilizing the big-M method [45], λ is a sufficiently large constant. The constraint in (12a) guarantees the earliest time that an FBS k can start serving at CP i ; e_0 is the mission start time of an FBS k at the BS. Also, t_{ij} denotes the travel time from BS i to CP j , i.e., the link between vertices. The constraint in (12b) ensures the timeline in which the FBS k arrives at CP j after arriving at CP i , serving in the service time s and traveling from the CP i to the CP j . Furthermore, s_i denotes the service time at CP i . The constraint in (12c) ensures that an FBS k returns to the BS before the maximum window time l_0 . Note that the constraints in (12a)–(12c) guarantee no subtours [46] discussed by Miller-Tucker-Zemlin (MTZ) formulation [47]. The constraints in (12d)–(12e) allow to obtain the accurate arrival time of FBSs at each CP. With the accurate arrival time of FBSs at CPs, overlap among serving FBSs can be detected in the time domain. The constraint in (12f) guarantees that GUs at CP i are served by an FBS within the time window, i.e., QoS support.

Based on the above constraints, a mathematical program for the FBS path planning with time windows and the UDG model in a single-cell network, which is also called optimal UAV trajectory planning in a single-cell network (OUT-S), is formulated as follows,

$$(P1), \text{ OUT-S: } \min_{\mathbf{W}, \mathbf{X}} \sum_{k \in \mathcal{K}} \sum_{i \in \mathcal{V}} \sum_{\substack{j \in \mathcal{V} \\ (i \neq j)}} t_{ij} x_{ijk} \quad (13)$$

$$\text{s. t.: } (11a)–(11d), (12a)–(12f),$$

$$x_{ijk} \in \{0, 1\}, \quad \forall k \in \mathcal{K}, \quad \forall i, j (i \neq j) \in \mathcal{V}, \quad (14)$$

$$w_i \geq 0, \quad \forall i \in \mathcal{V}_c, \quad (15)$$

where $\mathbf{W} \triangleq \{w_i | \forall i \in \mathcal{V}_c\}$, $\mathbf{X} \triangleq \{x_{ijk} | \forall i, j \in \mathcal{V}, \forall k \in \mathcal{K}\}$. The goal of OUT-S is to minimize total travel time (TTT) for all FBS's trajectories. Then, in order to create the multi-cell use case with predefined cell boundaries, the decision variable x should be revisited because it cannot support a link (route) that belongs to a specific cell [1], i.e., a feasible link in a cell with boundary. Therefore, we adopt the set of an auxiliary variable denoted as $\mathbf{Q} \triangleq \{q_{ijc} | \forall i, j \in \mathcal{V}, \forall c \in \mathcal{C}\}$ as given by,

$$\mathbf{Q} = \begin{bmatrix} q_{111} & q_{121} & \dots \\ \vdots & \ddots & \\ q_{i11} & & q_{ij1} \end{bmatrix}^c, \quad (16)$$

which creates feasible or infeasible FBS routes in the given cell. This represents either feasible routes or infeasible routes, i.e., if a link between vertex i and vertex j is within a given cell c , then $q_{ijc} = 1$, otherwise $q_{ijc} = 0$.

By adding this variable, we formulate an FBSs path planning formulation with time windows in a multi-cell network allowing for coverage and boundary of the given cell as a MILP mathematical program. In this case, the FBS path is estimated by defining a decision variable z as given by,

$$z_{ijk} = \begin{cases} 1, & \text{if an FBS } k \text{ uses a link between vertex } i \text{ and} \\ & \text{vertex } j \text{ within a boundary of cell,} \\ 0, & \text{otherwise.} \end{cases} \quad (17)$$

Hence, the CPs and the BS are separated in each set C_m , $m \in \mathcal{V}_d$. The adjusted multi-cell setting optimization problem can now be formulated as follows.

$$(P2): \min_{\mathbf{W}, \mathbf{X}, \mathbf{Z}} \sum_{k \in \mathcal{K}} \sum_{i \in \mathcal{V}} \sum_{\substack{j \in \mathcal{V} \\ (i \neq j)}} t_{ij} z_{ijk} \quad (18)$$

$$\text{s. t.: } (11a)–(11d), (12a)–(12f), (14)–(15),$$

$$z_{ijk} = x_{ijk} \cdot q_{ijc}, \quad \forall k \in \mathcal{K}, \quad \forall i, j (i \neq j) \in \mathcal{V}, \quad \forall c \in \mathcal{C}, \quad (19)$$

$$z_{ijk} \in \{0, 1\}, \quad \forall k \in \mathcal{K}, \quad \forall i, j (i \neq j) \in \mathcal{V}, \quad (20)$$

where $\mathbf{Z} \triangleq \{z_{ijk} | \forall i, j \in \mathcal{V}, \forall k \in \mathcal{K}\}$. We note that since the constraint in (19) is obviously non-linear, the problem (P2) is a MINLP that is thus difficult to be solved directly. Therefore, this constraint is required to be transformed by exploiting an elimination of products technique [40] as given by,

$$z_{ijk} \leq x_{ijk}, \quad \forall k \in \mathcal{K}, \quad \forall i, j (i \neq j) \in \mathcal{V}, \quad (21a)$$

$$z_{ijk} \leq q_{ijc}, \quad \forall k \in \mathcal{K}, \quad \forall i, j (i \neq j) \in \mathcal{V}, \quad \forall c \in \mathcal{C} \quad (21b)$$

$$z_{ijk} \geq x_{ijk} + q_{ijc} - 1, \quad \forall k \in \mathcal{K}, \quad \forall i, j (i \neq j) \in \mathcal{V}, \quad \forall c \in \mathcal{C}. \quad (21c)$$

By replacing the constraint in (19) with the constraints in (21a)–(21c), the novel optimization problem with linearization, which is also called optimal UAV trajectory planning in a multi-cell network (OUT-M), is formulated as follows,

$$(P3), \text{ OUT-M: } \min_{\mathbf{W}, \mathbf{X}, \mathbf{Z}} \sum_{k \in \mathcal{K}} \sum_{i \in \mathcal{V}} \sum_{\substack{j \in \mathcal{V} \\ (i \neq j)}} t_{ij} z_{ijk} \quad (22)$$

$$\text{s. t.: } (11a)–(11d), (12a)–(12f), (14)–(15), (20), (21a)–(21c),$$

$$\sum_{k \in \mathcal{K}} \sum_{i \in \mathcal{V}} \sum_{\substack{j \in \mathcal{V} \\ (i \neq j)}} z_{ijk} = N + K, \quad (23)$$

$$\forall k, K \in \mathcal{K}, N \in \mathcal{V}_c, \forall i, j (i \neq j) \in \mathcal{V}.$$

The goal of OUT-M is to minimize the TTT for all FBS's trajectories. The OUT-M corresponds to optimizing an FBS trajectory only feasible to fly over each given cell. In the problem OUT-M, the constraint in (23) activates links (routes) of the variable z in the network, the number of which is equal to the summation of both the number of CPs (N) and the number of FBSs (K).

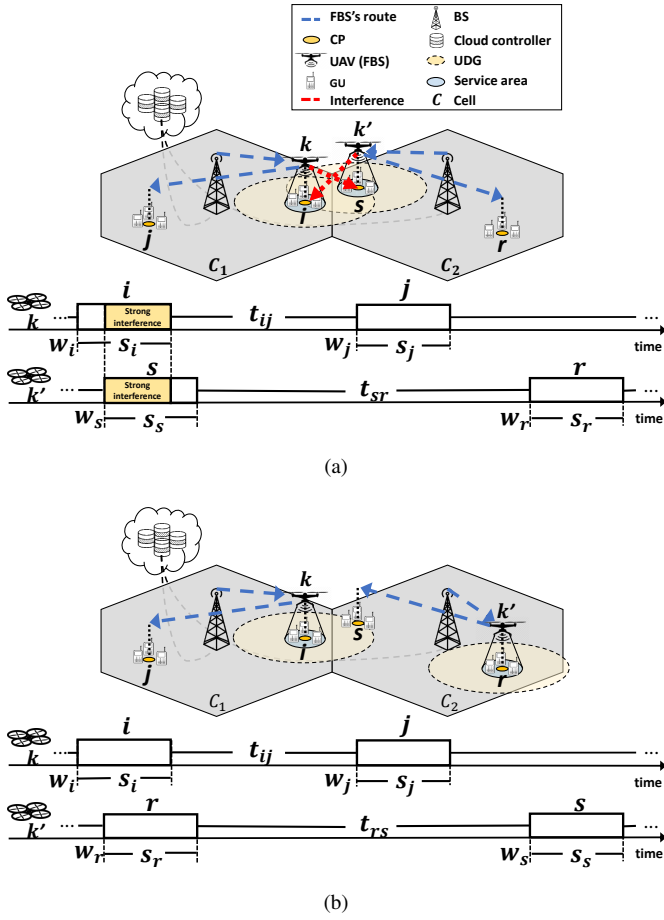


Fig. 3. An example of the scenario for a multi-cell network with two UAVs (FBSs) and four CPs. (a) Strong interference occurred between FBS k and k' at CP i and CP s respectively. The UDGs of the FBSs detected the strong interference when the CPs served by the FBSs are within the range of UDGs. (b) Both FBS k and k' with the UDG were aware of the strong interference and traveled to different paths compared to the paths in Fig. 3(a) in order to avoid the interference, i.e., the FBS k' arrived at the CP r first instead of arriving at the CP s first.

B. Interference-Aware UAV Trajectory Planning Formulation with Time Window under UDG Model

It is worth emphasizing that the above optimal solutions are oblivious to the effects of strong co-channel interference that might be caused by when multiple FBSs visit CPs and serve GUs in close proximity, which has detrimental effects on the achievable data rate for the transmission. An example of such potential occurrence is shown in Fig. 3(a). As can be seen from the figure, there is an overlap on the time domain when FBSs k and k' visit those two CPs (i and s) fell within the UDG range which also means in close proximity. Therefore, in order to avoid the interference, we propose an FBS interference-aware path planning optimization design with the UDG model to increase overall network performance in terms of the achievable throughput.

To this end, based on the defined preliminaries with the decision variables described in (9), (10), and (17), we addi-

tionally define a decision variable y as follows,

$$y_{ij} = \begin{cases} 1, & \text{if CP } i \text{ is served and then CP } j \text{ is served} \\ & \text{under UDG,} \\ 0, & \text{otherwise,} \end{cases} \quad (24)$$

where $i, j (i \neq j) \in \psi_h$, $\psi_h \in \Psi$, in which $\Psi = \{\psi_1, \dots, \psi_r\}$ and ψ denotes two different CPs that fall within the interference range with the UDG model and hence the two CPs cannot be served simultaneously if they are in close proximity. Thus, the proposed interference-aware FBS path planning formulation with the UDG model and time windows in a single-cell network follows the ones detailed in the previous section with the addition of the following constraints, which is called optimal UAV trajectory planning in a single-cell network with interference awareness (OUT-SIA).

$$(P4), \text{ OUT-SIA: } \min_{\mathbf{W}, \mathbf{X}, \mathbf{Y}} \sum_{k \in \mathcal{K}} \sum_{i \in \mathcal{V}} \sum_{\substack{j \in \mathcal{V} \\ (i \neq j)}} t_{ij} x_{ijk} \quad (25)$$

$$\text{s. t.: } (11a)-(11d), (12a)-(12f), (14)-(15),$$

$$y_{ij} = 1 - y_{ji}, \quad \forall i, j (i \neq j) \in \psi_h, \quad \psi_h \in \Psi, \quad (26)$$

$$w_i + s_i \leq w_j + M(1 - y_{ij}), \quad (27)$$

$$\forall i, j (i \neq j) \in \psi_h, \quad \psi_h \in \Psi,$$

$$y_{ij} \in \{0, 1\}, \quad \forall i, j (i \neq j) \in \psi_h, \quad \psi_h \in \Psi, \quad (28)$$

where $\mathbf{Y} \triangleq \{y_{ij} \mid \forall i, j \in \psi_h\}$. The goal of OUT-SIA is to minimize the TTT for all FBSs trajectories. The constraint in (26) ensures that if the variable y_{ij} is 1, then the y_{ji} is 0 and vice versa. The constraint in (27) ensures that if the variable y_{ij} is 1, then the service at CP i without overlap of the service at CP j under the UDG is guaranteed. The constraint in (28) represents that the variable y is binary.

We also propose an interference-aware FBS path planning formulation with the UDG model and time windows in a multi-cell network, which is also called Optimal UAV Trajectory planning in a Multi-cell network with Interference Awareness (OUT-MIA), as follows,

$$(P5), \text{ OUT-MIA: } \min_{\mathbf{W}, \mathbf{X}, \mathbf{Y}, \mathbf{Z}} \sum_{k \in \mathcal{K}} \sum_{i \in \mathcal{V}} \sum_{\substack{j \in \mathcal{V} \\ (i \neq j)}} t_{ij} z_{ijk} \quad (29)$$

$$\text{s. t.: } (11a)-(11d), (12a)-(12f), (14)-(15), \\ (20), (21a)-(21c), (23), (26)-(28).$$

The goal of OUT-MIA is to minimize the TTT for all FBSs trajectories. The OUT-x⁶ (S/M) is only able to detect where the interference occurs with the UDG model. However, as depicted in the Fig. 3(b), the OUT-MIA is aware of the area and avoid the epicenter where more than two FBSs are simultaneously served in close proximity using the UDG model, and exploits the additional constraints in (26)–(28) to enforce non-overlapping service times on the time domain. In other words, FBSs with the UDG will in turn change their route to avoid the strong interference in the OUT-xIA

⁶The term 'x' represents both the single-cell indicated by 'S' and the multi-cell indicated by 'M'.

Algorithm 1 HUT-x**Input:** Parameters in Table II**Output:** TTT, AAT, \mathbb{U} , \mathbb{E}

```

1:  $\Theta \leftarrow$  Parameters in Table II
2: Initialize cells setting according to  $M$ , and allocate all
   CPs and BSs
3:  $Rt(\Theta) \leftarrow$  Generate routes based string consisting of CPs
   ( $N$ ) and BSs ( $M$ ), and then randomly divide the route
   into the number of FBSs ( $K$ )
4:  $\Delta \leftarrow$  Compute  $Time\ cost\{Rt(\Theta)\}$ 
5: for  $T := 0$  to  $I_t$  do
6:    $\Gamma \leftarrow$  Randomly select a scheme in LST // 2-Opt,
     Relocate, Swap and Randomization [16], [41]
7:    $Rt'(\Theta) \leftarrow$  Execute LST $\{Rt(\Theta), \Gamma\}$  and update the
     routes
8:    $\mathcal{H}(j) \leftarrow$  Detect interference level in different CPs //
      $\mathcal{H}(j) \in \{0, 1\}, \forall j \in \mathcal{V}_c$ 
9:    $\Delta' \leftarrow$  Compute a new  $Time\ cost\{Rt'(\Theta)\}$ 
10:  if  $\Delta' < \Delta$  then
11:     $Rt \leftarrow Rt'$ 
12:     $\Delta \leftarrow \Delta'$ 
13:  end if
14:   $I_t \leftarrow I_t - 1$ 
15: end for
16: return  $Rt, \Delta, \mathcal{H}(j)$ 

```

(SIA/MIA). For example, as shown in Fig. 3(b), the FBS k' travels to the CP r for the service instead of traveling towards the CP s .

IV. PROPOSED SET OF HEURISTIC ALGORITHMS

In this section, we propose both a local search heuristic under the UDG model and an interference-aware local search heuristic under the UDG model, which are called a Heuristic UAV Trajectory planning in single/multi-cell network (HUT-x (S/M)) algorithm and a Heuristic UAV Trajectory planning with Interference-Aware in single/multi-cell network (HUT-xIA (SIA/MIA)) algorithm respectively, as a scale-free one in order to tackle the curse of dimensionality of the underlying optimization problems. The pseudo codes are summarized in Alg. 1 and Alg. 2 respectively. Both heuristic algorithms take interference into consideration by using the UDG model. Also, they exploit the well-known LST, i.e., 2-Opt, Relocate, Swap and Randomization [16], [41], which is appropriate to finding the lowest cost for path planning. The HUT-x only detects interference that cooperatively occurs between FBSs, while the HUT-xIA is aware of the interference and capable of avoiding it. The LST provides FBS routes, which consists of a set of strings of numbers, with a mixture described in [1].

The HUT-xIA iteratively creates string-based FBSs route by using the LST while maintaining avoidance of interference in Repeat-Until loop represented in the Step 6–16 of Alg. 2 until $\text{sum}(\mathcal{H}(j)) == 0$ converges. In the loop, if the distance between CP i and j (to be served by each FBS) is shorter than the UDG range θ_r , then $\mathcal{J}(i, j) = 1$, otherwise, $\mathcal{J}(i, j) = 0$. With $\mathcal{J}(i, j) = 1$, if the FBS k' serves GUs at CP j while

Algorithm 2 HUT-xIA**Input:** Parameters in Table II**Output:** TTT, AAT, \mathbb{U} , \mathbb{E}

```

1:  $\Theta \leftarrow$  Parameters in Table II
2: Initialize cells setting according to  $M$ , and allocate all
   CPs and BSs
3:  $Rt(\Theta) \leftarrow$  Generate routes based string consisting of CPs
   ( $N$ ) and BSs ( $M$ ), and then randomly divide the route
   into the number of FBSs ( $K$ )
4:  $\Delta \leftarrow$  Compute  $Time\ cost\{Rt(\Theta)\}$ 
5: for  $T := 0$  to  $I_t$  do
6:   Repeat
7:    $\Gamma \leftarrow$  Randomly select a scheme in LST // 2-Opt,
     Relocate, Swap and Randomization [16], [41]
8:    $Rt'(\Theta) \leftarrow$  Execute LST $\{Rt(\Theta), \Gamma\}$  and update the
     routes
9:    $\mathcal{J}(i, j) \leftarrow$  Compute the Euclidean distance between
     CPs,  $\mathcal{J}(i, j) \in \{0, 1\}, \forall i, j \in \mathcal{V}_c$  // If  $\mathcal{J}(i, j) < \theta_r$ ,
     then 1, otherwise 0
10:   $w(i, k) \leftarrow$  Compute the arrival time of UAV  $k$  at CP  $i$ 
     with exploiting  $Rt', \forall k \in \mathcal{K}$ 
11:  if  $\mathcal{J}(i, j) == 1$  then
12:    if  $w(i, k) \leq w(j, k') \ \&\& \ w(j, k') \leq w(i, k) + s_i$ ,
        $\forall k' \in \mathcal{K} \setminus \{k\}$  then
13:       $\mathcal{H}(j) \leftarrow 1$  // Interference occurrence,  $\mathcal{H}(j) \in$ 
         $\{0, 1\}, \forall j \in \mathcal{V}_c$ 
14:    end if
15:  end if
16:  Until  $\text{sum}(\mathcal{H}(j)) == 0$ 
17:   $\Delta' \leftarrow$  Compute a new  $Time\ cost\{Rt'(\Theta)\}$ 
18:  if  $\Delta' < \Delta$  then
19:     $Rt \leftarrow Rt'$ 
20:     $\Delta \leftarrow \Delta'$ 
21:  end if
22:   $I_t \leftarrow I_t - 1$ 
23: end for
24: return  $Rt, \Delta$ 

```

the FBS k is already serving GUs at CP i , then $\mathcal{H}(j) = 1$, otherwise $\mathcal{H}(j) = 0$. Hence, the loop is repeated until the summation of the $\mathcal{H}(j)$ is equal to zero, i.e., interference does not occur at all CPs. Once the loop achieves convergence that creates FBSs routes (paths) with minimizing interference, the final FBSs routes are constructed. Then, the whole process is repeated by the iteration number I_t and the best path is adopted in greedy manner. To this end, the goal of the algorithm is to improve the total cost in order to find competitive paths with minimization of interference in the case of proximate FBSs.

V. NUMERICAL INVESTIGATIONS

In this section, we provide a wide set of numerical investigations by Monte Carlo simulations to evaluate the performance of the proposed schemes compared to previously proposed techniques by operating with Intlinprog solver in MATLAB.

Table II summarizes system model parameters that have been used for the simulations. We vary the number of CPs

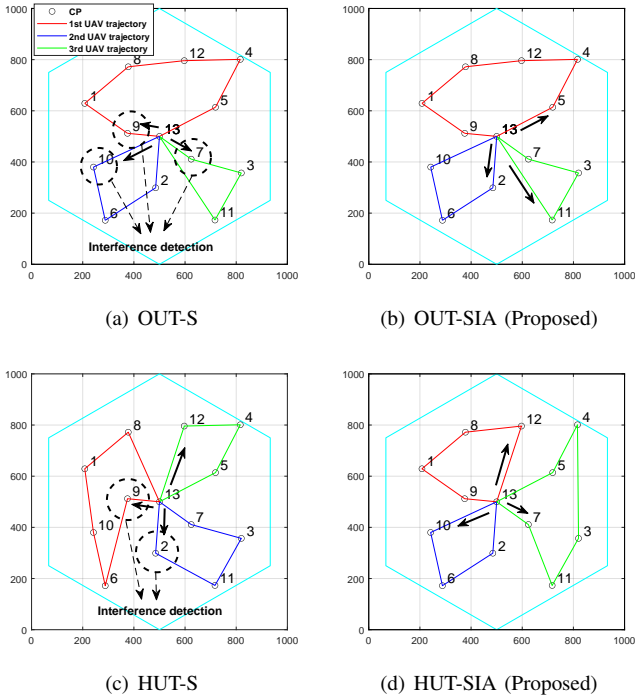


Fig. 4. An example of FBS trajectories for approaches in a single-cell.

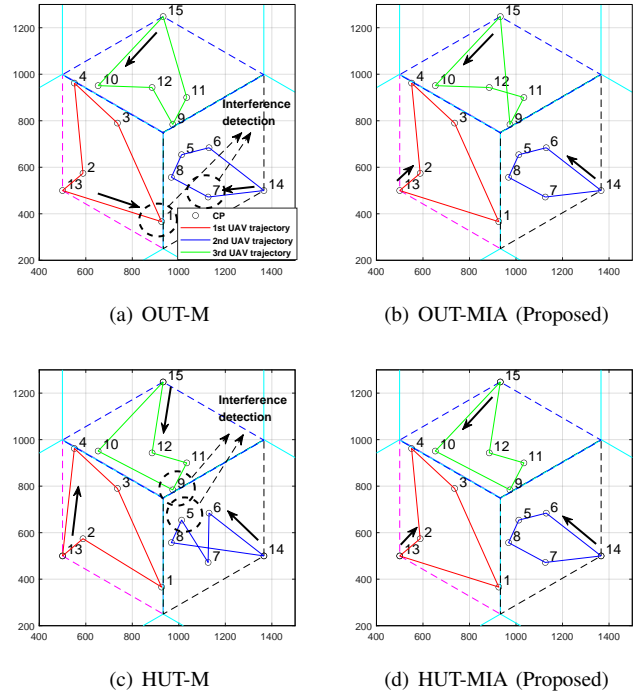


Fig. 5. An example of FBS trajectories for approaches in a multi-cell.

TABLE II
SIMULATION PARAMETERS.

Parameter	Value
Cell radius	500 m
Number of FBSs (K)	3
Number of CPs (N)	9, 12, 15, 18
Number of BSs (M)	1, 3
Location of CPs	random distribution
Velocity of FBSs (v)	10.21 m/s [19]
Altitude of FBSs (h)	100 m
GU location (R)	20 m [44]
UDG range (θ_r)	250, 300, 350 m
Mission start/maximum time (e_0, l_0)	0, 5000 s
Service time (s)	20 s
$\alpha, \beta, \xi_{\text{LoS}}, \xi_{\text{NLoS}}$	9.6, 0.28, 1, 20 [44]
Carrier frequency (f_c)	2 GHz [42]
Transmit power of FBS (P_t)	23 dBm [48]
Noise power (\mathcal{N}_0)	-120 dBm
SINR threshold (γ_{th})	10 dB [44]
Iteration numbers (I_t)	5000

(N), BSs (M) and the radius θ_r of the UDG model. The CPs incorporating a cluster of GUs are randomly distributed in a large predefined geographical area, i.e., a single-cell and a multi-cell with the cell radius. In the multi-cell, it is worth noticing that the CPs are only distributed in inter-cell areas getting involved at the edge of the cells in the case of high competition of FBS's service (as shown in Fig. 5).

We adopt an UAV modelled with rotary wings [19]. In [19], the UAV with rotary wings is deployed with two components of energy consumption, i.e., traveling energy and hovering energy. Moreover, the authors [19] derived the optimal velocity of the UAV that minimizes the energy consumption while maximizing the UAV endurance. This modeling can be applied to our system. Therefore, we assume the velocity v of the FBS

is the optimal value, i.e., 10.21 m/s (further details can be seen in [19, Fig. 2]).

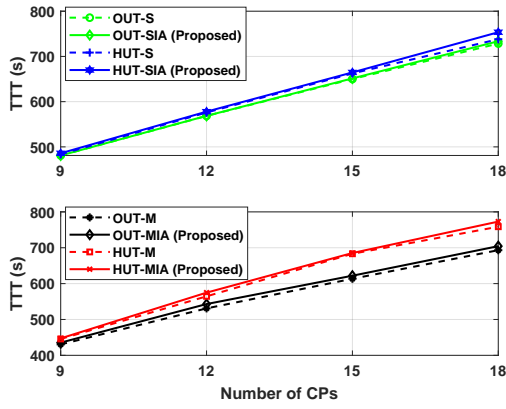
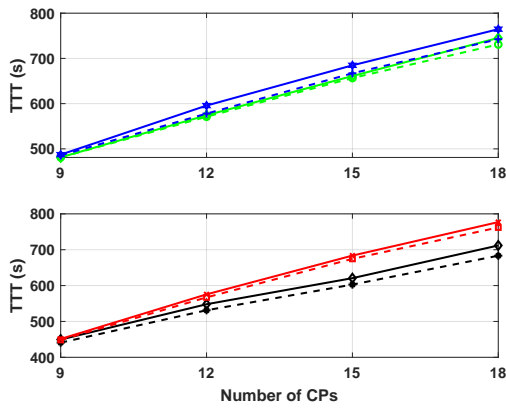
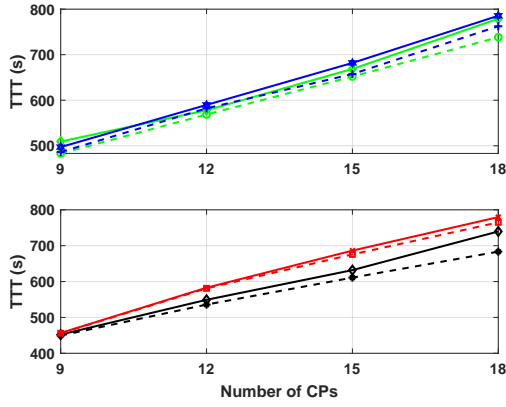
Without loss of generality, the value of the service time⁷ s at the CPs (i.e., $s_i \triangleq s$), the altitude h , the transmit bandwidth B , the transmit power P_t and carrier frequency f_c of all FBSs are assumed to be identical. Moreover, the number of FBSs (K) are fixed to three as multiple FBSs⁸. The parameterization of $\alpha, \beta, \xi_{\text{LoS}}$ and ξ_{NLoS} is selected so as to represent a typical urban environment, and the SINR threshold γ_{th} is set to 10 dB [44]. Setting an appropriate UDG radius depends on the SINR requirements and hereafter we detail how the SINR requirements are linked with selecting a range θ_r for the UDG radius. To this end, in order for $\text{SINR}_{i,k} > \gamma_{\text{th}}$ at each CP, we set the UDG range θ_r as 250 to 350m, i.e., $\theta_r > \arg \min_{d_{ij}} (\text{SINR}_{i,k} > \gamma_{\text{th}}), \forall i, j \in \mathcal{V}_c$.

We compare the proposed approaches OUT-xIA and HUT-xIA, which are enabled to be aware of interference, with two baselines which are described below,

- **OUT-x (S/M):** These schemes have been developed as both the optimal solution (P1) and (P3) in the Section III-A. They are oblivious of interference, which means that FBSs are not able to avoid strong interference when multiple FBSs simultaneously serve in proximity.

⁷Typically, the service time is considered as a random variable (in most cases an exponential distribution is used and an assumption comes back from the days of telephony). We decided to avoid including another level of randomization from the outset in the numerical investigations so that we flesh out the gains of the proposed solutions in a clearer manner. In essence, we assume a constant service time s that is equal to the mean value of a given exponential function.

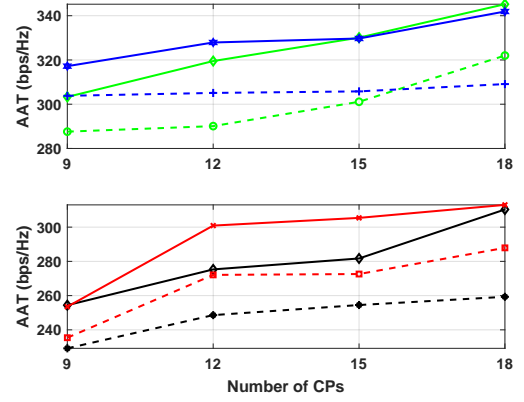
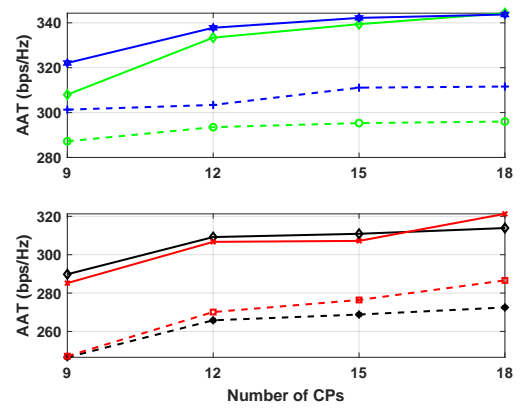
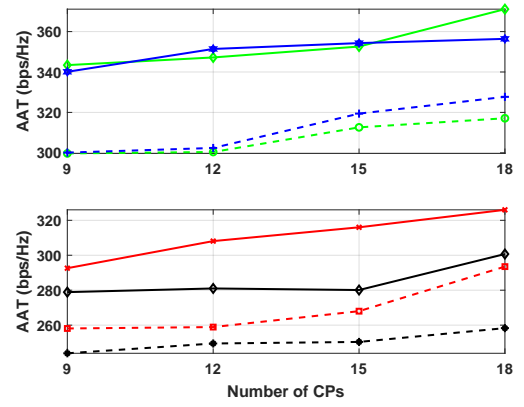
⁸The simulation is stopped at 120 minutes running time, which is the case when the following parameters were combined and exceeded these values: $N > 18, K > 3, \theta_r > 350$.

(a) TTT, $\theta_r = 250$ (b) TTT, $\theta_r = 300$ (c) TTT, $\theta_r = 350$ Fig. 6. Total traveling time (TTT) with varying θ_r and N .

However, they are still able to detect the interference under the UDG model.

- **HUT-x (S/M):** These schemes are the local search heuristic algorithm summarized in Alg. 1 based on state of the art techniques, i.e., the LST, [16], [41], which also operates in the same manner as OUT-x.

We note that from the baseline schemes mentioned above, the OUT-S and the HUT-S schemes resemble the widely used conventional schemes, i.e., the single-cell setting and the UAV deployment returning to an original depot without explicitly

(a) AAT, $\theta_r = 250$ (b) AAT, $\theta_r = 300$ (c) AAT, $\theta_r = 350$ Fig. 7. Average achievable throughput (AAT) with varying θ_r and N .

taking into account interference as well as considering a multi-cell wireless network [17], [22].

A. FBS Trajectory Analysis

Figs. 4 and 5 illustrate examples of nominal FBSs trajectories with the parameters $K = 3$, $N = 12$, and $\theta_r = 300$ for all different schemes in a single-cell ($M = 1$) and a multi-cell ($M = 3$) network scenario. Note that the numbers 13, 14, and 15 represent macro BSs that act as depots which are the locations where the FBSs depart and return. The black arrows

represent directions of the FBSs and the black dotted circles indicate the spots where interference is detected. To provide a more in-depth analysis in Fig. 5, we zoomed in the edges of the three hexagon cells where FBSs of adjacent BSs are located in close proximity, hence representing the worst-case interference scenario. We note that the OUT-xIA and HUT-xIA schemes manage to completely avoid the interference under the UDG model, while the OUT-x and the HUT-x schemes that are interference-oblivious (i.e., the first without the constraints in (26)–(28) and the second without the Repeat-Until loop in the Steps 6–16 of Alg. 2) cannot eliminate rendezvous points of FBSs (i.e., FBSs in close proximity), hence allowing high levels of interference as shown in Figs. 4 and 5.

Specifically, both the OUT-x and HUT-x schemes create a few areas where strong interference is taking place as depicted by the black dotted circles. Whereas, observe that for the proposed OUT-xIA and HUT-xIA schemes, there are no areas of strong interference (i.e., no rendezvous points) and it is also interesting to notice that the two proposed schemes minimize the interference even though the FBSs utilize different trajectories; in other words, they manage to find paths without increasing total travel time (TTT) in order to provide strong interference avoidance in the network.

B. TTT and AAT Performance

Figs. 6 and 7 show TTT and AAT with respect to the different size of θ_r of UDG and the number of N for all schemes. In general, as the number of N is increased, AAT of the proposed OUT-xIA and HUT-xIA turn significantly higher than that of two baselines, OUT-x and HUT-x. Specifically, the gain of AAT of OUT-SIA obtained is around 15.7% when $\theta_r = 350$, $N = 18$ compared to the OUT-S and the gain of AAT of OUT-MIA obtained is around 14.9% when $\theta_r = 300$, $N = 9$ compared to the OUT-M. Similarly, the AAT of HUT-SIA gained about 14.6% when $\theta_r = 300$, $N = 18$ compared to the OUT-S and the AAT of HUT-MIA gained approximately 20.8% when $\theta_r = 350$, $N = 15$ compared to the HUT-M. In terms of TTT, all schemes generally gained similar values, which means that the overall energy consumption of the FBS is not increased since the majority of it is consumed for the traveling time [10], [19]. The TTT of the multi-cell is generally higher than that of the single-cell as the FBS trajectory is less flexible to be changed in the multi-cell network. Furthermore, as expected, the TTT of HUT-xIA was slightly higher than that of OUT-xIA since HUT-SIA and HUT-MIA are suboptimal solutions.

As the size of θ_r is increased, the gain of AAT of all the proposed solutions is generally also increased. Whereas, the computational time of the proposed optimal solutions is exponentially climbed (this is represented in Section V-D). It is interesting to notice that a few of cases of the AAT of HUT-xIA are higher than that of OUT-xIA, e.g., $\theta_r = 250, 350$, since the underlying focus is on the objective with minimizing the FBS's traveling time. Whereas, the TTT of HUT-xIA is always greater than OUT-SIA since HUT-xIA is in essence suboptimal solutions to the objective.

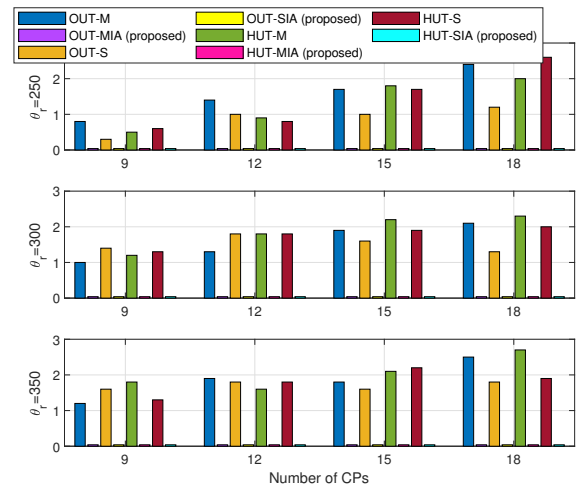


Fig. 8. Interference detection (\mathbb{U}) versus the number of CPs (N) according to θ_r for all schemes. The vertical axis represents the value of \mathbb{U} defined in the Section V-C.

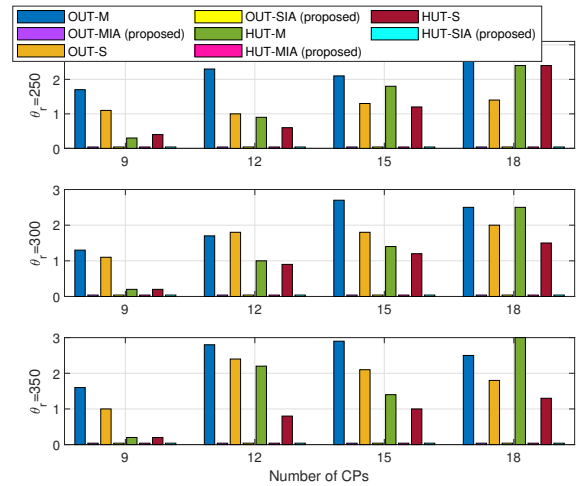


Fig. 9. Outage event (\mathbb{E}) versus the number of CPs (N) according to θ_r for all schemes. The vertical axis represents the value of \mathbb{E} defined in the Section V-C.

C. Interference Detection and Outage Events

In this subsection, we focus on the number of interference detection events under the UDG model (ID-UDG) per a mission where all FBSs return to the BS as well as provide an analysis of outage events (OE) where the SINR value is compared with γ_{th} in each CP. These metrics are measured using the following binary variables,

$$\text{ID-UDG}_i = \begin{cases} 1, & \text{if UDG with } \theta_r \text{ of an FBS at CP } i \text{ incor-} \\ & \text{porates other different UDGs of FBSs} \\ & \text{at CPs when to serve simultaneously,} \\ 0, & \text{otherwise,} \end{cases} \quad (30)$$

$$\text{OE}_i = \begin{cases} 1, & \text{if } \text{SINR}_i < \gamma_{th}, \\ 0, & \text{otherwise,} \end{cases} \quad (31)$$

TABLE III
COMPARISON BETWEEN ALL APPROACHES ON COMPLEXITY AND SCALABILITY.

	Parameter				Number of variables	Number of constraints	Computational complexity	Computation time (s)
	K	N	M	θ_r				
OUT-S	3	9	1	250	309	320	NP-hard	5.3
	3	18	1	250	1101	959	NP-hard	9.8
	3	9	1	350	309	320	NP-hard	5.3
	3	18	1	350	1101	959	NP-hard	16.7
OUT-M	3	9	3	250	873	2112	NP-hard	19.3
	3	18	3	250	2664	6045	NP-hard	263.9
	3	9	3	350	873	2112	NP-hard	22.8
	3	18	3	350	2664	6045	NP-hard	284.2
OUT-SIA (Proposed)	3	9	1	250	390	482	NP-hard	5.9
	3	18	1	250	1425	1607	NP-hard	4225.4
	3	9	1	350	390	482	NP-hard	857.4
	3	18	1	350	1425	1607	NP-hard	6887.8
OUT-MIA (Proposed)	3	9	3	250	954	2436	NP-hard	19.1
	3	18	3	250	2988	7341	NP-hard	577.3
	3	9	3	350	954	2436	NP-hard	22.0
	3	18	3	350	2988	7341	NP-hard	4975.9
HUT-S	3	9	1	250	n/a	n/a	$\mathcal{O}(I_t N K (N + K)^2)$	3.3
	3	18	1	250	n/a	n/a	$\mathcal{O}(I_t N K (N + K)^2)$	4.9
	3	9	1	350	n/a	n/a	$\mathcal{O}(I_t N K (N + K)^2)$	4.0
	3	18	1	350	n/a	n/a	$\mathcal{O}(I_t N K (N + K)^2)$	7.8
HUT-M	3	9	3	250	n/a	n/a	$\mathcal{O}(I_t N K (N + K)^2)$	2.9
	3	18	3	250	n/a	n/a	$\mathcal{O}(I_t N K (N + K)^2)$	5.0
	3	9	3	350	n/a	n/a	$\mathcal{O}(I_t N K (N + K)^2)$	3.9
	3	18	3	350	n/a	n/a	$\mathcal{O}(I_t N K (N + K)^2)$	6.1
HUT-SIA (Proposed)	3	9	1	250	n/a	n/a	$\mathcal{O}(I_t N K (N + K)^2 \zeta)$	5.8
	3	18	1	250	n/a	n/a	$\mathcal{O}(I_t N K (N + K)^2 \zeta)$	8.3
	3	9	1	350	n/a	n/a	$\mathcal{O}(I_t N K (N + K)^2 \zeta)$	8.5
	3	18	1	350	n/a	n/a	$\mathcal{O}(I_t N K (N + K)^2 \zeta)$	14.1
HUT-MIA (Proposed)	3	9	3	250	n/a	n/a	$\mathcal{O}(I_t N K (N + K)^2 \zeta)$	5.1
	3	18	3	250	n/a	n/a	$\mathcal{O}(I_t N K (N + K)^2 \zeta)$	12.2
	3	9	3	350	n/a	n/a	$\mathcal{O}(I_t N K (N + K)^2 \zeta)$	19.5
	3	18	3	350	n/a	n/a	$\mathcal{O}(I_t N K (N + K)^2 \zeta)$	38.1

where $\forall i \in \mathcal{V}_c$. Hence, \mathbb{U} , which is defined as the number of ID-UDG, can be given by,

$$\mathbb{U} = \sum_{i=1}^N \text{ID-UDG}_i, \quad (32)$$

where $\mathbb{U} \leq N$. In the similar way, \mathbb{E} , which is defined as the number of OE, can be expressed as,

$$\mathbb{E} = \sum_{i=1}^N \text{OE}_i, \quad (33)$$

where $\mathbb{E} \leq N$.

Figs. 8 and 9 describe \mathbb{U} and \mathbb{E} respectively according to the size of θ_r and N for all schemes. It is clear that the proposed OUT-xIA and HUT-xIA manage to construct FBS paths with no UDG-based interference, i.e., $\mathbb{U} = 0$, and achieve a SINR greater than the γ_{th} value, i.e., $\mathbb{E} = 0$, in the entire simulations. Moreover, it is noticeable that the \mathbb{U} and the \mathbb{E} values of the OUT-x and the HUT-x have an upward trend as the size of θ_r is increasing. Note that the \mathbb{U} and the \mathbb{E} values of the OUT-M and HUT-M are slightly greater than those of the OUT-S and the HUT-S in general. This is because in the multi-cell scenario, the number of FBSs rendezvous points is increasing and as a result the number of strong interference events is expected to increase.

D. Scalability and Complexity Analysis

We present performance comparison between the optimal solutions and the proposed algorithms in network instances

where optimal solutions could be achieved. The computational dimensionality of the optimization problems is as follows,

- **OUT-S:** $|\mathcal{V}| + 2|\mathcal{V}_c| + |\mathcal{V}_d| + |\mathcal{K}| |\mathcal{V}| + 4|\mathcal{K}| |\mathcal{V}_c| |\mathcal{V}_d| + 2|\mathcal{V}_c|^2 + |\mathcal{K}| |\mathcal{V}|^2$
- **OUT-M:** $|\mathcal{V}| + 2|\mathcal{V}_c| + |\mathcal{V}_d| + |\mathcal{K}| |\mathcal{V}| + 4|\mathcal{K}| |\mathcal{V}_c| |\mathcal{V}_d| + 2|\mathcal{V}_c|^2 + 3|\mathcal{K}| |\mathcal{V}|^2 + 2|\mathcal{K}| |\mathcal{C}| |\mathcal{V}|^2 + |\mathcal{K}| |\mathcal{V}_c| |\mathcal{V}|^2$
- **OUT-SIA:** $|\mathcal{V}| + 2|\mathcal{V}_c| + |\mathcal{V}_d| + |\mathcal{K}| |\mathcal{V}| + 4|\mathcal{K}| |\mathcal{V}_c| |\mathcal{V}_d| + 2|\mathcal{V}_c|^2 + |\mathcal{K}| |\mathcal{V}|^2 + 3|\Psi|^2$
- **OUT-MIA:** $|\mathcal{V}| + 2|\mathcal{V}_c| + |\mathcal{V}_d| + |\mathcal{K}| |\mathcal{V}| + 4|\mathcal{K}| |\mathcal{V}_c| |\mathcal{V}_d| + 2|\mathcal{V}_c|^2 + 3|\mathcal{K}| |\mathcal{V}|^2 + 2|\mathcal{K}| |\mathcal{C}| |\mathcal{V}|^2 + |\mathcal{K}| |\mathcal{V}_c| |\mathcal{V}|^2 + 3|\Psi|^2$.

These cause substantial increase in the search space, resulting in significant difficulty to obtain optimal solutions for medium to large network instances. Table III shows the effect of parameters K , N , M , and θ_r on the complexity and scalability of the simulations. Note the exponential growth of both the decision variables and the number of constraints. However, in terms of the complexity, the HUT-x and the proposed HUT-xIA have $\mathcal{O}(I_t N K (N + K)^2)$ and $\mathcal{O}(I_t N K (N + K)^2 \zeta)$, respectively, which are simply yielded by parameters I_t , K , N and ζ . Specifically, N , K , and I_t of the complexity represent the effect of the iterations and $(N + K)^2$ represents the worst case complexity of the LST algorithm, i.e., 2-Opt, in the Alg. 1 and Alg. 2. We note that ζ denotes one iteration of the Repeat-Until loop given in the Steps 6–16 in Alg. 2. A wide set of investigations for the Alg. 2, i.e., HUT-xIA, reveal that we can reach convergence with only few iterations (less than 20 on average in the simulations) and in a computational efficient

manner, i.e., 0.5 ms to 5 ms⁹. This implies that a network orchestrator can compute the trajectories of the multiple FBSs in real-time.

In general, since OUT-x and OUT-xIA are in the category of NP-hard (the proof can be seen in the Appendix VI), they require significant higher computational time compared to the HUT-x and HUT-xIA solutions as shown in Table III. Furthermore, the computational time for all solutions has, as expected, a growing trend as the parameters of the network instance increase. To this end, observe that the OUT-xIA scheme is experiencing the highest computational complexity. On the other hand, a key aspect worth pointing out is that both the proposed HUT-xIA algorithms provide competitive solutions in low computation time for large network instances, rendering them amenable for real-time implementation. It is also worth noticing that the computation time of the proposed HUT-SIA is much lower than that of the OUT-SIA, which attained nearly 488.5 times in computational reduction when $K = 3$, $N = 18$, $M = 1$, $\theta_r = 350$. Similarly, the computation time of the proposed HUT-MIA is approximately 130.6 times faster than that of the OUT-MIA, when $K = 3$, $N = 18$, $M = 3$, $\theta_r = 350$. Therefore, by accepting a minimal loss of the network capacity (i.e., optimality of the solution), the performance of both greedy and iterative HUT-xIA algorithms can be deemed as acceptable.

VI. CONCLUSIONS

This paper presents an interference-aware path planning optimization model under Hamiltonian paths with adjustable time windows to allow service differentiation for multiple UAVs operating as flying base stations (FBSs) deployed from a single or multiple macro-BSs acting as their depots in a single or multi-cell mobile network. A key innovative aspect is that the proposed optimization schemes modeled by MILP formulations and the associated heuristic algorithms incorporate the unit disk graph (UDG) interference model to enable interference avoidance in a highly scale free manner and by doing so they provide FBSs trajectories that minimize aggregate co-channel interference between different serving FBSs, translating in an increased aggregate network capacity. A wide set of numerical investigations reveal that the proposed solutions allow for approximately 21% gains (with 50% maximum gains) in the average achievable throughput (AAT) as well as enabling real-time implementation and low control plane overhead due to the use of the UDG model, whilst being able to maintain a similar level of total traveling time (TTT) compared to interference-oblivious solutions (which means that the overall energy consumption in the network is not increased).

The proposed set of solutions have a number of implications in the orchestration of FBSs in beyond 5G networks. We have shown that the interference-aware trajectory planning design can reduce rendezvous points of FBSs and therefore ease aggregate strong interference resulting in simpler and more

efficient closed-loop power control schemes to be utilized as constraints. Moreover, the proposed set of schemes can be included as scalable algorithms in network orchestration procedures related to UAV-aided beyond 5G networks in order to enable an efficient integration of aerial platforms with the fixed network infrastructure.

APPENDIX A

PROOF OF NP-HARDNESS

Lemma 1. *OUT-x and OUT-xIA are NP-hard problems.*

Proof. Recall that the constraints (11a)–(11c) capture the FBSs trajectory route constraints, whilst the constraints (12a)–(12c) ensure that a Hamiltonian cycle is created via sub-tour elimination. Therefore, if we eliminate the time window constraints the problem reduces to the TSP since the objective function seeks for paths with minimal aggregate total travel time. Hence, the underlying optimization problem resembles the conventional VRP and the minimum cost tour concept of TSP. Therefore, both the OUT-x and OUT-xIA optimization problems, as presented in the form of an MILP, encapsulate a TSP-like tour in terms of trajectory planning and as a result they are as hard as the TSP problem and therefore fall into the well-known NP-hard [23] set of problems. \square

REFERENCES

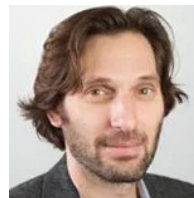
- [1] J. Lee and V. Friderikos, "Path optimization for flying base stations in multicell networks," in *Proc. IEEE WCNC*, 2020.
- [2] M. Giordani and M. Z^Morzi, "Non-terrestrial networks in the 6G era: Challenges and opportunities," *IEEE Netw.*, vol. 35, no. 2, pp. 244–251, 2020.
- [3] F. Nait-Abdesselam *et al.*, "Towards enabling unmanned aerial vehicles as a service for heterogeneous applications," *J. Commun. Netw.*, vol. 23, no. 3, 2021.
- [4] M. Giordani *et al.*, "Toward 6G networks: Use cases and technologies," *IEEE Commun. Mag.*, vol. 58, no. 3, pp. 55–61, 2020.
- [5] Z. Zhang *et al.*, "6G wireless networks: Vision, requirements, architecture, and key technologies," *IEEE Veh. Technol. Mag.*, vol. 14, no. 3, pp. 28–41, 2019.
- [6] A. Islam and S. Y. Shin, "Bus: A blockchain-enabled data acquisition scheme with the assistance of UAV swarm in Internet of things," *IEEE Access*, vol. 7, pp. 103231–103249, 2019.
- [7] A. Islam *et al.*, "A blockchain-based artificial intelligence-empowered contagious pandemic situation supervision scheme using Internet of drone things," *IEEE Wireless Commun.*, vol. 28, no. 4, 2021.
- [8] I. Bor-Yaliniz and H. Yanikomeroglu, "The new frontier in RAN heterogeneity: Multi-tier drone-cells," *IEEE Commun. Mag.*, vol. 54, no. 11, pp. 48–55, 2016.
- [9] S. Hayat, E. Yanmaz, and R. Muzaffar, "Survey on unmanned aerial vehicle networks for civil applications: A communications viewpoint," *IEEE Commun. Surveys Tuts.*, vol. 18, no. 4, pp. 2624–2661, Apr. 2016.
- [10] B. Li, Z. Fei, and Y. Zhang, "UAV communications for 5G and beyond: Recent advances and future trends," *IEEE Internet Things J.*, vol. 6, no. 2, pp. 2241–2263, 2018.
- [11] Y. Zeng, J. Lyu, and R. Zhang, "Cellular-connected UAV: Potential, challenges, and promising technologies," *IEEE Wireless Commun.*, vol. 26, no. 1, pp. 120–127, 2018.
- [12] V. Sharma *et al.*, "Intelligent deployment of UAVs in 5G heterogeneous communication environment for improved coverage," *J. Netw. Comput. Applicat.*, vol. 85, pp. 94–105, 2017.
- [13] H. Shakhateh *et al.*, "On the continuous coverage problem for a swarm of UAVs," *IEEE Sarnoff Symp.*, pp. 130–135, 2016.
- [14] Y. Li and L. Cai, "UAV-assisted dynamic coverage in a heterogeneous cellular system," *IEEE Netw.*, vol. 31, no. 4, pp. 56–61, 2017.
- [15] M. Erdelj *et al.*, "UAVs that fly forever: Uninterrupted structural inspection through automatic UAV replacement," *Ad Hoc Netw.*, vol. 94, Nov. 2019.

⁹We ran a personal computer with Intel i5-4690@3.5GHz and 16GB RAM in the simulation.

- [16] K. Dorling *et al.*, "Vehicle Routing Problems for Drone Delivery," *IEEE Trans. Syst., Man, Cybern., Syst.*, vol. 47, no. 1, pp. 70–85, Jan. 2017.
- [17] J. Yao and N. Ansari, "QoS-aware rechargeable UAV trajectory optimization for sensing service," in *Proc. IEEE ICC*, 2019.
- [18] Y. Zeng, X. Xu, and R. Zhang, "Trajectory design for completion time minimization in UAV-enabled multicasting," *IEEE Trans. Wireless Commun.*, vol. 17, no. 4, pp. 2233–2246, Apr. 2018.
- [19] Y. Zeng, J. Xu, and R. Zhang, "Energy minimization for wireless communication with rotary-wing UAV," *IEEE Trans. Wireless Commun.*, vol. 18, no. 4, pp. 2329–2345, 2019.
- [20] W. Chiang *et al.*, "Impact of drone delivery on sustainability and cost: Realizing the UAV potential through vehicle routing optimization," *Appl. Energy*, vol. 242, pp. 1164–1175, 2019.
- [21] W. P. Coutinho, M. Battarra, and J. Fliege, "The unmanned aerial vehicle routing and trajectory optimisation problem, a taxonomic review," *Comput. Ind. Eng.*, vol. 120, pp. 116–128, 2018.
- [22] C. Zhan and Y. Zeng, "Completion time minimization for multi-UAV-enabled data collection," *IEEE Trans. Wireless Commun.*, vol. 18, no. 10, pp. 4859–4872, 2019.
- [23] C. H. Papadimitriou, "The euclidean travelling salesman problem is NP-complete," *Theoretical Computer Science*, vol. 4, no. 3, pp. 237–244, 1977.
- [24] L. Xie, J. Xu, and Y. Zeng, "Common throughput maximization for UAV-enabled interference channel with wireless powered communications," *IEEE Trans. Commun.*, vol. 68, no. 5, pp. 3197–3212, 2020.
- [25] Q. Wu, Y. Zeng, and R. Zhang, "Joint trajectory and communication design for multi-UAV enabled wireless networks," *IEEE Trans. Wireless Commun.*, vol. 17, no. 3, pp. 2109–2121, 2018.
- [26] A. Rahmati *et al.*, "Interference avoidance in UAV-assisted networks: Joint 3D trajectory design and power allocation," in *Proc. IEEE GLOBECOM*, 2019.
- [27] C. Shen *et al.*, "Multi-UAV interference coordination via joint trajectory and power control," *IEEE Trans. Signal Process.*, vol. 68, pp. 843–858, 2020.
- [28] U. Challita, W. Saad, and C. Bettstetter, "Interference management for cellular-connected UAVs: A deep reinforcement learning approach," *IEEE Trans. Wireless Commun.*, vol. 18, no. 4, pp. 2125–2140, 2019.
- [29] M. M. U. Chowdhury *et al.*, "3-D trajectory optimization in UAV-assisted cellular networks considering antenna radiation pattern and backhaul constraint," *IEEE Trans. Aerosp. Electron. Syst.*, vol. 56, no. 5, pp. 3735–3750, 2020.
- [30] G. Zhu *et al.*, "Mission time minimization for multi-UAV-enabled data collection with interference," in *Proc. IEEE WCNC*, IEEE, 2021.
- [31] S. Zhang *et al.*, "Power control and trajectory planning based interference management for UAV-assisted wireless sensor networks," *IEEE Access*, vol. 8, pp. 3453–3464, 2019.
- [32] W. Mei, Q. Wu, and R. Zhang, "Cellular-connected UAV: Uplink association, power control and interference coordination," *IEEE Trans. Wireless Commun.*, vol. 18, no. 11, pp. 5380–5393, 2019.
- [33] I. Valilahi and C. Masouros, "Multi-UAV deployment for throughput maximization in the presence of co-channel interference," *IEEE Internet Things J.*, 2020.
- [34] E. Lebhar and Z. Lotker, "Unit disk graph and physical interference model: Putting pieces together," *IEEE Int. Symp. Parallel Distrib. Process.*, pp. 1–8, 2009.
- [35] Y. Zhu and H. Zheng, "Understanding the impact of interference on collaborative relays," *IEEE Trans. Mobile Comput.*, vol. 7, no. 6, pp. 724–736, 2008.
- [36] Q. Chen *et al.*, "Low-latency data aggregation scheduling for cognitive radio networks with non-predetermined structure," *IEEE Trans. Mobile Comput.*, 2020.
- [37] F. Cheng *et al.*, "UAV trajectory optimization for data offloading at the edge of multiple cells," *IEEE Trans. Veh. Technol.*, vol. 67, no. 7, pp. 6732–6736, Jul. 2018.
- [38] Y. Ji *et al.*, "Multicell edge coverage enhancement using mobile UAV-relay," *IEEE Internet Things J.*, vol. 7, no. 8, pp. 7482–7494, 2020.
- [39] C. Liu, K.H. Ho, and J. Y. Wu, "MmWave UAV networks with multi-cell association: Performance limit and optimization," *IEEE J. Sel. Areas Commun.*, vol. 37, no. 12, pp. 2814–2831, 2019.
- [40] H. P. Williams, *Model building in mathematical programming*, John Wiley & Sons, 2013.
- [41] T. Caric and H. Gold, *Vehicle Routing Problem*, London, U.K.: IntechOpen, ISBN: 978-953-7619-09-1, 2008.
- [42] A. Al-Hourani, S. Kandeepan, and A. Jamalipour, "Modeling air-to-ground path loss for low altitude platforms in urban environments," in *Proc. IEEE GLOBECOM*, 2014.
- [43] A. Al-Hourani, S. Kandeepan, and S. Lardner, "Optimal LAP altitude for maximum coverage," *IEEE Wireless Commun. Lett.*, vol. 3, no. 6, pp. 569–572, 2014.
- [44] M. Mozaffari *et al.*, "Drone small cells in the clouds: Design, deployment and performance analysis," in *Proc. IEEE GLOBECOM*, 2015.
- [45] D. Bertsimas and J. N. Tsitsiklis, *Introduction Linear Optim.*, vol. 6, 1997.
- [46] U. Pferschy and R. Stanek, "Generating subtour elimination constraints for the TSP from pure integer solutions," *Central Eur. J. Operations Research*, vol. 25, no. 1, pp. 231–260, 2017.
- [47] I. Kara, G. Laporte, and T. Bektas, "A note on the lifted Miller–Tucker–Zemlin subtour elimination constraints for the capacitated vehicle routing problem," *Eur. J. Operational Research*, vol. 158, no. 3, pp. 793–795, 2004.
- [48] 3GPP, "Technical Specification Group Radio Access Network; Study on New Radio (NR) to support non-terrestrial networks," 3GPP Technical Report, Sep. 2020.



Jongyul Lee received the M.Sc. degree in Electronic and Computing Engineering from Hanyang University, Republic of Korea, in 2016, and he is currently pursuing the Ph.D. degree from 2018 in the Centre for Telecommunications Research (CTR) at King's College London, the United Kingdom. His research interests include UAV-aided network, Vehicular network, and wireless mobile networks. The emphasis of his research is network optimization for path planning and resource allocation in wireless networks.



Vasilis Friderikos is currently a Reader at the Department of Engineering at King's College London. He was a Visiting Researcher at Rutgers University, New Jersey, USA and a Visiting Lecturer at the Institut Supérieur de l'Electronique et du Numérique, France, in 2010. He has authored more than 200 research papers in flagship IEEE, Elsevier, Springer journals, international conferences, and book chapters, and also holds patents. His research interests lie broadly within the closely overlapped areas of wireless networking, mobile computing, and architectural aspects of the future Internet. The emphasis of his research is the design and analysis of algorithms for caching, routing, admission control, load, and power management in virtualized wired-cum wireless networks, with application to both centralized and distributed implementations. He is a member of IEEE, the IET and the INFORMS section on Telecommunications. He was a recipient of the British Telecom Fellowship Award in 2005. He received the Best Paper Award from the IEEE ICC 2010 Conference and the WWRF Conference. He was a Program Co-Chair of IEEE ICT 2016 and a Co-Chair of the IEEE WCNC 2010 Conference (acting as a Technical Program Committee Member of the IEEE GLOBECOM, IEEE ICC, and several other flagship international conferences). He was also an organizing committee member of the Green Wireless Communications and Networks Workshop (GreenNet) of VTC Spring 2011 and Workshop co-chair of the IEEE International Conference on Pervasive Intelligence and Computing, 2022.